Hindawi
Shock and Vibration
Volume 2022, Article ID 3639936, 18 pages
https://doi.org/10.1155/2022/3639936

Research Article

Seismic Performance of Concrete-Filled Square Steel Tubular Column-Steel Beam Sleeve Joint

Xiangong Huang,[1] Man Xu,[1] Nan Guo,[1] Senwen Deng,[2] and Le Huang[3]

[1]*School of Civil Engineering, Northeast Forestry University, Harbin 150000, China*
[2]*School of Civil Engineering, Heilongjiang University, Harbin 150000, China*
[3]*Ping'an Construction Group Co., Ltd., Hangzhou 310000, China*

Correspondence should be addressed to Man Xu; xuman306@126.com

Received 13 August 2021; Accepted 7 June 2022; Published 19 July 2022

Academic Editor: Manuel Aenlle Lopez

The concrete-filled square steel tubular (S-CFST) structure has been widely used as a resistance system against earthquakes due to its good seismic performance. However, the application of the S-CFST structure is limited by its complex joint formulation. To overcome this shortcoming, a sleeve semirigid joint has been proposed, while its seismic performance has not been well examined. This study aims to discuss the behavior of sleeve joints with different parameters under low cyclic loading. The analysis results show that the simulation results of the finite element model established by ABAQUS were in good agreement with the experimental results, which further verified the good energy dissipation performance of the sleeve joint, and gave the design suggestions of the joint under different parameters to promote the engineering application of this type of joint.

1. Introduction

The concrete-filled steel tube (CFST) has various advantages, such as high bearing capacity, good plasticity and toughness, easy processing, and convenient construction [1, 2]. However, the complexity of the design and construction of beam-column joints limits its application to some extent. In addition, almost all current joints are designed as rigid joints, but the semirigid joint under the action of cyclic loading shows a better energy dissipation performance and more stable seismic characteristics, which has attracted extensive attention of researchers [3–8].

In recent years, researchers have conducted plenty of research on the types and mechanical properties of semirigid joints of concrete-filled steel tubes, and some achievements have been made. For example, Oh and Ai-Roda [9] carried out an experimental study on the connection of concrete-filled steel tubular column and H-shaped steel beam. T-cleat connections and bending steel plates with a centered hole were used to strengthen the stiffness of the connection, and the hysteretic performance of the connection was analyzed. It was found that the joint of bending steel plates with a centered hole demonstrates good deformation ability. Ricles et al. [10] conducted low reversed cyclic loading tests on 10 full-scale joints of concrete-filled square steel tubular (CFST) column and steel beam. They found that the flange joints of the T-shaped steel bolt connection and reinforced beam meet the design principle of "strong column and weak beam," and the bolted end-plate connection can enhance the bolt hole strength, effectively reducing the slippage and the pinch phenomenon of hysteretic curves. Yang et al. [11] studied the mechanical properties of joints through diaphragms of concrete-filled rectangular steel tubular column and H-shaped steel plate under low cyclic loading. The results showed that such type of joint has good seismic performance, and the wedge-shaped plates on both sides of the flange have a significant influence on the joint ductility. Lv and Li [12] proposed a joint form with an octagonal ring beam outside the CFST column and designed three specimens to study its mechanical properties. The obtained results indicated that the three specimens all show high bearing capacity, good ductility, and energy dissipation

capacity under cyclic loading. Mirza and Uy [13] used the experiment and finite element method to study the performance of bolted beams, columns, and horizontal end-plate joints. The mechanical properties of flat end joints of the composite beam-column under low-probability, high-consequence loading were investigated. Gao et al. [14] researched the mechanical characteristics and energy dissipation performance of different forms of large-size connections of CFST column and H-shaped steel beam. He concluded that the bearing capacity and energy dissipation performance of joints with inner diaphragms are better than those of joints with through diaphragms. France and Buick Davison [15] carried out static loading tests on the bolted end-plate joint of CFST column and steel beam and compared its performance with that of the square steel tubular column joint. Through experimental analysis, it was found that the strength and stiffness of the joint are significantly improved, but the joint ductility is reduced, and the failure mode of the joint is bolt pull out.

For the simulation model and calculation theory of the concrete-filled steel tube column-steel beam semirigid joint, the research focus is mainly on the connection with bolts, and the deformation model of the connection element is established. Huang [16] used ABAQUS to establish two-element connectors to simulate the beam-column joint used in the bolted end-plate connection. Compared with the experiment data, this finite element model (FEM) effectively simulated the force exerted on the joint under high temperatures. In such conditions, the axial force of the beam end has an obvious influence on the force exerted on the joint. Hu et al. [17] studied the performance of T-shaped steel bolted joints under low cyclic loading and proposed a new mechanical calculation model for such joints. The model diagram is shown in Figure 1, where the mechanical model simulated T-shaped steel as a nonlinear spring element, and a multiline segment cyclic stiffness model was used to simulate the hysteretic performance of T-shaped steel components. By comparing the simulated results of this model with the experimental results, it was concluded that this model can accurately simulate the mechanical behavior of T-shaped steel bolted joints [17].

Many achievements have been obtained in the connection test and theoretical study of semirigid joints of CFST column and steel beam, but the existing semirigid joint forms have their own limitations. It is difficult to find a joint form with both technical and economic advantages; thus, it is necessary to select the suitable joint type based on the application situation by developing the advantages and avoiding the disadvantages. In this paper, the sleeve joint form of concrete-filled square steel tubular column-steel beam was studied, and its mechanical properties under low cyclic loading are investigated using ABAQUS. This joint is shown in Figure 2.

2. Model Design

The sleeve joint is formed by sheathing the steel sleeve at the joint position of concrete-filled square steel tubular column, welding the upper and lower edges of the sleeve with the steel tubular column, and then completely welding the steel beam with the sleeve, and the joint has clear force transmission and simple construction. To investigate the seismic performance of concrete-filled square steel tubular column-steel beam sleeve joint, three joint models of this type are designed.

2.1. Model Dimension. Three sleeve joint specimens of CFST column and steel beam, numbered from CFST-1 to CFST-3, were designed. The size of the square steel tubular column was 300 × 300 × 8 mm (length × width × thickness), and the steel beams were made of HN244 × 175 × 7 × 11 mm hot-rolled H-beam. Strength grade Q235 steel was used for beams, columns, and sleeves, and concrete with strength grade C30 was filled in the square steel tube. The sleeve was welded with steel plates, and the type of electrode was E43. The upper and lower flanges and web at one end of the steel beam were completely welded on the sleeve. A 5 mm weld was left on the top and bottom of the sleeve to weld the sleeve on the square steel tubular column, the periphery of which was in full contact with the square steel tubular column. The variables were the thickness and height of the sleeve. The main parameters are shown in Table 1, and the detailed joint structure is shown in Figure 3.

2.2. Material Properties. Steel is simulated by the conventional ideal elastic-plastic model, and Q235 steel was adopted in this model, with an elastic modulus of $E = 2.03 \times 10^5$ N/mm^2, a Poisson ratio of 0.3, and a density of 78.5 g/mm^2.

The concrete constitutive model is the plastic damage model of square steel tubes proposed by Han et al. [18, 19], which considers the interaction between the inner wall of square steel tube and core concrete.

3. Model Validation

3.1. Experimental Setup. Two MTS actuators were used to apply low cyclic load to the beam ends on both sides of the specimen, and the Jack on the column top was utilized to apply the axial force, while hinged supports were placed at the column bottom and column end to simulate the hinged boundary conditions. In the test, four H-shaped steel was installed as limit beams to ensure that the components do not have out-of-plane torsion and instability before failure and to limit the lateral displacement of the specimen during loading. It is specified in the test that the pushing direction of the actuator is positive and the pulling direction is negative, and the left and right beams were marked. During the test, firstly, a vertical axial force of 770 kN (axial compression ratio of 0.23) was applied on the column top with a Jack. Then, MTS actuators were utilized to apply displacement cyclic load on the left and right beam ends at the same time, with a displacement increment of 5 mm. When the specimen yielded, cyclic loading was continued three times with the same increment until any of the following conditions occurred: (1) the load is reduced to less than 80% of the peak load; (2) the steel tube in the joint area is locally damaged by

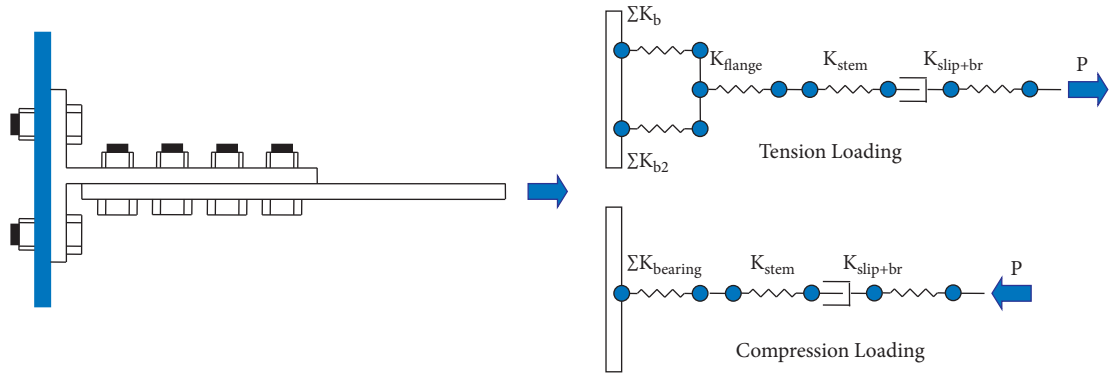

Figure 1: Hu calculation model.

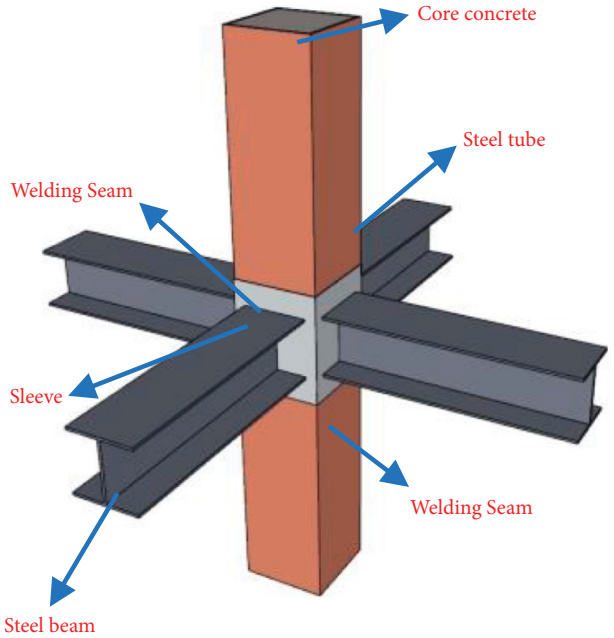

Figure 2: Sketch of sleeve joint.

Table 1: Sleeve parameters of specimens height × side length- × thickness (mm).

CFST-1	CFST-2	CFST-3
488 × 312 × 6	600 × 312 × 6	488 × 320 × 10

shear or more than 70% of the local weld cracks; (3) the steel beam has obvious local buckling deformation or fracture, or the steel beam has out-of-plane instability.

The stress distribution in the core area of the joint was measured by both the strain gauge and the stain rosette that are arranged according to Figure 4. The displacement of the beam end was measured by a displacement sensor and collected synchronously and automatically by a computer. The test device is shown in Figure 5. Due to the sticking and measurement, the strain gauge and the stain rosette did not work well, so the measurement results of strain were not provided in this paper.

3.2. Material Mechanical Properties

3.2.1. Steel. According to the provisions in metallic materials–tensile testing–method of test at ambient temperature (GB/T 228.1–2010) [20] and steel and steel products–location and preparation of samples and test pieces for mechanical testing (GB/T 2975–2018) [21], three groups with two samples per group from the same batch of steel were taken to conduct tensile tests on the material universal testing machine. The performance parameters measured are shown in Table 2.

3.2.2. Concrete. When pouring C30 concrete, three 150 × 150 × 150 mm standard concrete test cubes and three 150 × 150 × 300 mm prismatic blocks were fabricated. After 28 days of curing under the same conditions as the joint specimens, the compressive test on the concrete cube was carried out, and then the average value was taken. Ultimately, the measured average compressive strength of concrete cubes was 40.59 MPa, the average axial compressive strength was 27.18 MPa, and the average elastic modulus was 31783 MPa.

3.3. FE Model. Solid element C3D8R in ABAQUS is used to build the model, including steel beam, steel tube, core concrete, and steel sleeve. The mesh of the connection area is encrypted by using structured mesh and considering the complex stress and calculation accuracy of the connection area. The mesh size of the joint connection area between steel tube and beam is 15 mm, and the rest parts are 60 mm. Steel sleeve is the key component of joint connection, which is divided by 15 mm. The size of core concrete is 160 mm.

The normal attribute between steel pipe and concrete is "hard" contact, the tangential direction is defined as limited sliding, and the friction coefficient is 0.3. Except the weld joint area, the contact between the steel tube and the steel sleeve is defined as "hard," which means that there is no immersion between the two faces.

3.4. Failure Mode. The failure phenomena of the three specimens under different loading displacements are shown in Table 3, where 55 mm (1) represents the first circle load

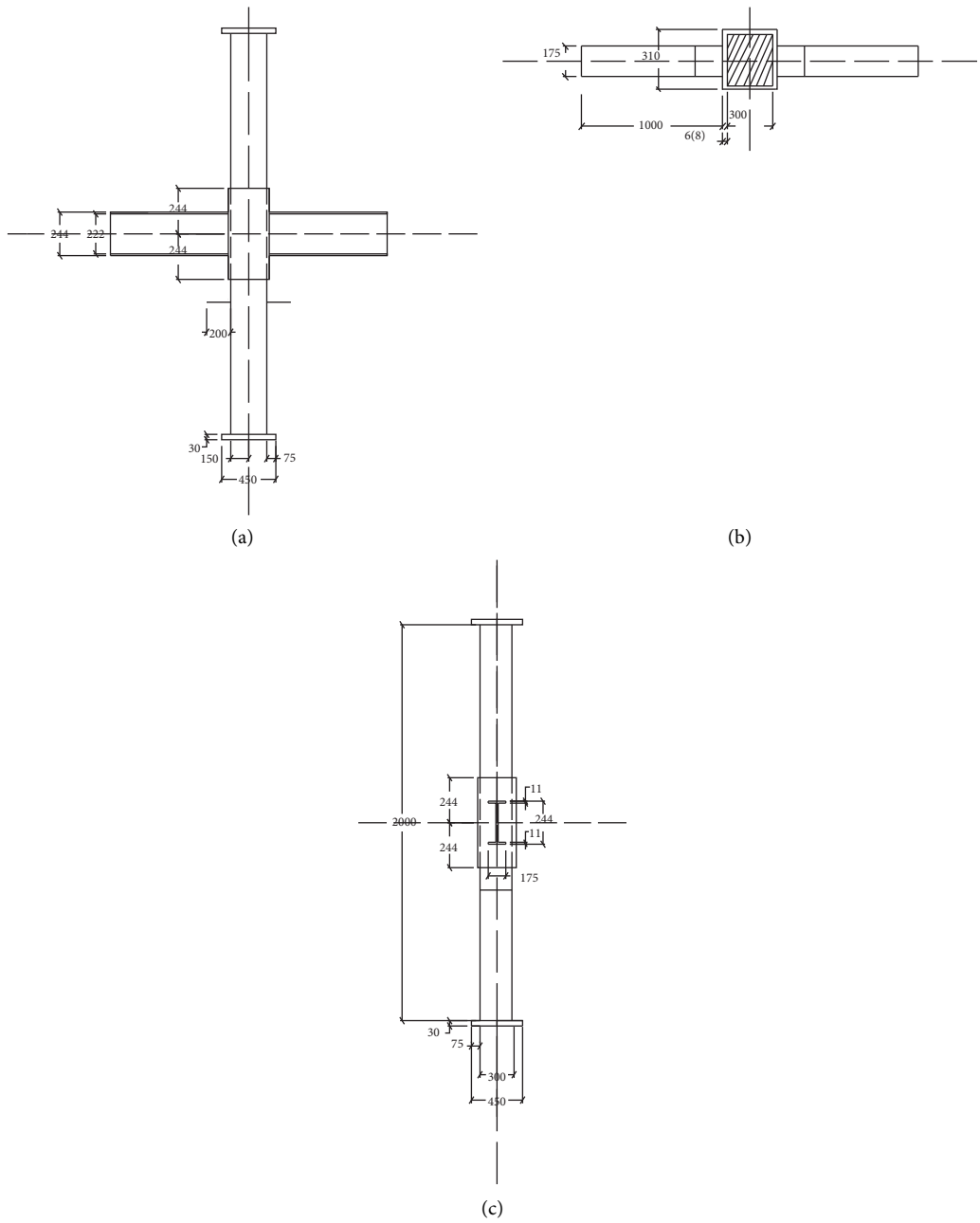

Figure 3: Detailed joint structure. (a) Elevation, (b) plan, and (c) profile.

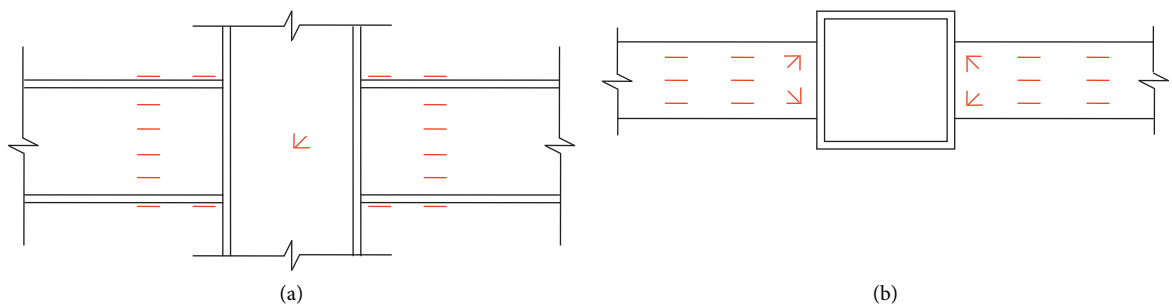

Figure 4: Strain gauge arrangement. (a) Front view and (b) top view.

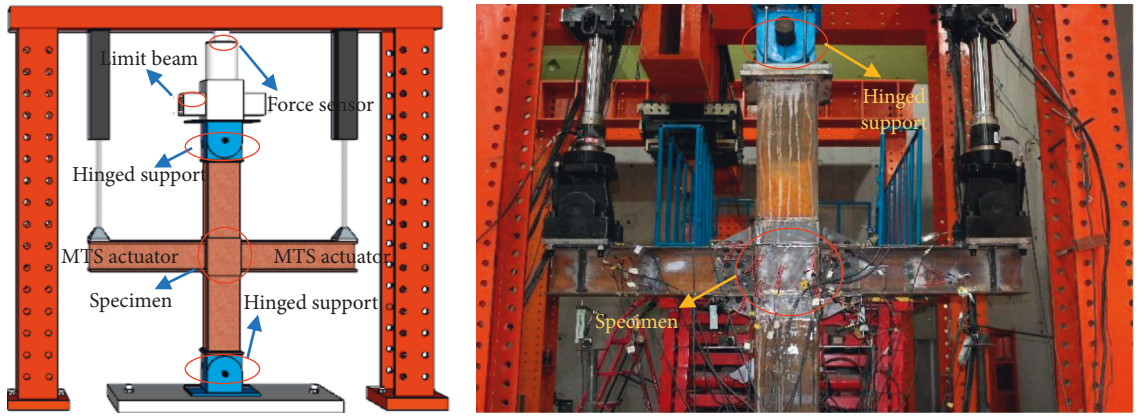

Figure 5: Diagram of the test device. (a) Model diagram and (b) physical diagram.

Table 2: Performance parameters of steel.

Thickness (mm)		Measured strength (MPa)		Average strength (MPa)
5.65	Yield strength	323.86	322.72	323.29
	Ultimate strength	474.09	473.42	473.76
7.65	Yield strength	299.50	282.88	291.19
	Ultimate strength	390.05	392.82	391.43
9.67	Yield strength	313.57	319.68	316.62
	Ultimate strength	420.86	427.45	424.15

Table 3: Failure phenomena of specimens.

No.	Vertical loading displacement	Failure phenomena
CFST-1	55 mm (1)	The upper flange of the right beam and the lower flange of the left beam have large local buckling
	55 mm (2)	The sleeve local buckling at the connection between the right beam and the sleeve and the left beam and the sleeve is about 15 mm and 20 mm, respectively
	55 mm (3)	The upper flange weld of the right beam and the lower flange weld of the left beam crack
	60 mm (1)	The base metals on the lower side of the right beam and the upper side of the left beam are torn
	60 mm (3)	The base metals on the upper and lower flanges are torn
	65 mm (2)	The connection between the sleeve and the upper flange and the sleeve and the lower flange of the right beam is torn about 30 mm and 8 mm, respectively; the connection between the sleeve and the upper flange of the left beam is torn about 40 mm
	65 mm (3)	The specimen failure occurs
CFST-2	55 mm (1)	The adhesion failure occurs between the concrete and steel tube wall
	60 mm (1)	The base metal on the lower flange of the right beam is torn
	60 mm (2)	The base metal on the upper flange of the left beam is torn, and the sleeve local buckling occurs
	65 mm (1)	The sleeve of the right beam has a tear of about 2 mm
	65 mm (2)	The upper flange of the left beam is partially separated from the sleeve
	65 mm (3)	The flange on both sides of the beam is separated from the sleeve, and specimen failure occurs
CFST-3	65 mm (1)	The upper flange of the right beam has a local buckling
	65 mm (2)	The sleeve of the left beam has a local buckling of about 8 mm
	65 mm (3)	The base metals on the lower side of the right beam and the upper side of the left beam are torn, and the sleeve of the left beam has a local buckling of about 12 mm
	70 mm (1)	The left beam is distorted
	70 mm (2)	The base metal has been torn, and the sleeve of the left beam has a crack of about 6 mm
	70 mm (3)	The sleeve of the left beam is slightly damaged and has a local buckling, and the whole weld is torn
	75 mm (2)	The flange on both sides of the beam is separated from the sleeve, and specimen failure occurs

when the displacement of the beam end is 55 mm. The failure modes of these specimens are shown in Figure 6.

The test phenomena, failure processes, and failure modes of three sleeve joint specimens were identical, belonging to the failure mode of semirigid joints with high stiffness. Therefore, the seismic performance of the joint can be improved by improving the design, welding process, and sequence or strengthening the strength check and quality inspection of the weld.

A full finite element model was built by ABAQUS as shown in Figure 7. The axial force was applied on the top of the column, and the cyclic load was applied on the beam end to simulate the test loading conditions. The displacement constraints in X and Y directions and rotation constraints in Y and Z directions were applied at the top of the column, and X, Y, Z displacement constraints and Y, Z rotation constraints were imposed at the bottom of the column.

Figure 8 shows the comparison of joint failure modes of specimen CFST-1 between the simulated results and experimental results. It can be seen from the figure that the simulation failure mode of the sleeve joint is almost the same as the experimental result. The failure mode of the specimen is mainly the buckling and the tearing of the sleeve. However, because the material damage is not given in the material property, the tearing of the sleeve is not simulated in the finite element model. The place where the joint deformation is large is the place where the steel is torn. The ABAQUS finite element model established in this paper can accurately simulate the failure mode of joints.

Figure 9(a) shows the stress distribution of the steel beam. It can be seen from the figure that the flange of the beam is curved. This phenomenon also occurs in the specimen CFST-1, the sleeve buckling is obvious, and the flange of the beam is easier to bend. It shows that the specimen with thinner sleeve wall thickness is more prone to buckling under the same axial compression ratio.

The finite element analysis can simulate the stress distribution of the steel tube column inside the sleeve, which cannot be obtained in the test. Figure 9(b) shows the stress distribution of steel tube under ultimate load. It can be seen that when the specimen was damaged, because the sleeve is only connected with the steel tube by the upper and lower welds, the corresponding part of the steel tube is also the part with the greatest stress in the loading process, and it is also the part most prone to deformation and buckling.

Figure 10 shows a comparison of failure modes between extended end-plate joints and sleeve joints. The extended end-plate joint is a typical semirigid joint [22, 23], and its main failure modes are shown in Figure 10(a). One kind of failure is that while the upper flange of the steel beam is taken as the rotation center, the end plate at the lower flange also has bending deformation, which is consistent with the failure mode of the sleeve joint. The other kind of failure is that the end plate below the upper flange of the steel beam is basically in a straight line; that is, the end plate has no obvious bending deformation, and the failure mode is consistent with the weld tearing failure mode of sleeve joint. From the analysis of rotation capacity and failure modes, the sleeve joint conforms to the connection characteristics of the semirigid joint.

3.5. Hysteretic Curve. The load-displacement hysteretic curves of the specimen beam end are shown in Figure 11, where the graph in the first and third quadrants is the hysteretic curve of the left beam end and the graph in the second and fourth quadrants is the hysteretic curve of the right beam end. Both graphs are shuttle-shaped, indicating good deformability, seismic performance, and energy dissipation capacity of the specimen. Since cyclic load is applied on both sides of the beam end, the corresponding hysteretic curves are symmetrically distributed. When the specimen reached the yield state, the hysteretic curve analysis showed that some specimens had buckled. After yielding, the first cyclic load value of each displacement level was higher than that of the next two cycles, indicating that the joint strength and stiffness degrade with loading. In terms of ultimate bearing capacity, specimen CFST-2 did not change much compared with specimen CFST-1, suggesting that increasing the sleeve height will not improve the bearing capacity. However, the area of hysteretic curves of specimen CFST-2 was larger than that of specimen CFST-1. It implicated that the energy dissipation capacity of joint specimen CFST-2 is higher than that of joint specimen CFST-1.

Figure 12 shows that the simulated hysteretic curve is in good agreement with the experimental curve, which verifies the rationality of the finite element method [24, 25]. The load value of the simulated hysteretic curve was slightly higher than that of the experimental hysteretic curve. This is because the finite element model ignores the influence of the weld quality between the sleeve and the flange of the steel beam as well as the environment of the specimen. The initial stiffness of the joint in the finite element analysis was larger than that in the test, which is because the weld of the specimen basically appears in the part where one end of the steel beam is connected with the sleeve, while the weld is not considered in the finite element analysis.

3.6. Skeleton Curve. When applying cyclic load on the steel beam end, the skeleton curve can be obtained by successively connecting the maximum load in each stage of the hysteretic curve. The skeleton curves of three joint specimens are shown in Figure 13. The skeleton curves of the joint specimen are basically S-shaped, and the sleeve joints undergo obvious elastic, elastic-plastic, and plastic failure processes during loading. However, the skeleton curves of the left and right beam ends are not completely symmetrical. This is because the quality of the welds on both sides of the beam end cannot be the same, and cumulative damage occurs at the joints. The initial stiffness, ultimate bearing capacity, and ultimate displacement of specimen CFST-3 were significantly higher than those of CFST-1 and CFST-2, indicating that increasing the sleeve thickness can effectively improve the seismic performance of the sleeve joint.

As shown in Figure 13, the simulated and experimental skeleton curves are both S-shaped, and the joint specimens

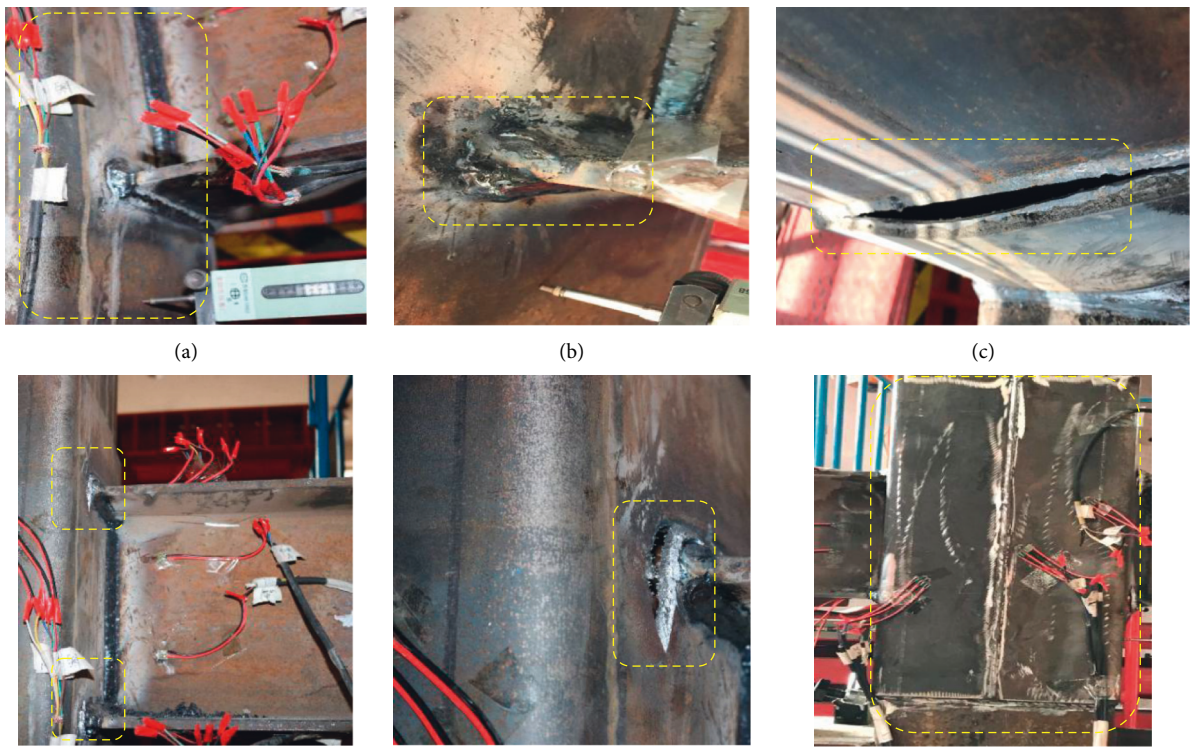

Figure 6: Failure modes of specimens. (a) Sleeve local buckling; (b) base metal tearing of the left; (c) weld cracking; (d) base metal tearing of upper; (e) sleeve tearing; (f) joint failure.

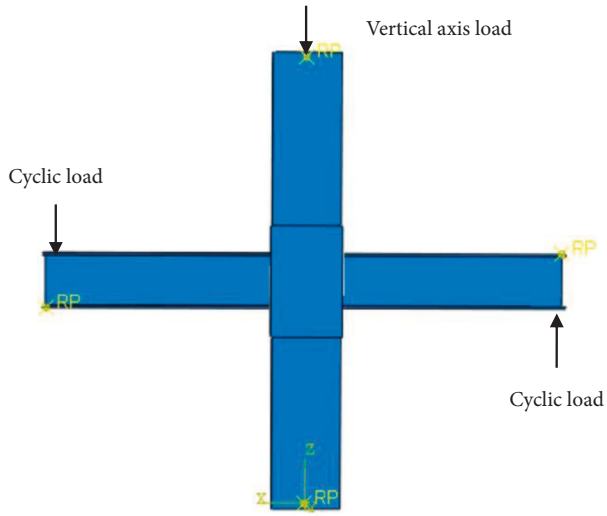

Figure 7: Loading conditions.

have experienced three stages under low cyclic loading, that is, elastic, elastic-plastic, and plastic failure. The simulated and experimental skeleton curves were also roughly consistent in values, with a load value error within 10%, which further illustrates the rationality of the finite element method. By comparison, the simulated skeleton curve using FEM is more symmetrical, but the symmetry of the experimental skeleton curve is slightly worse. This is because there was residual deformation during loading; thus, the skeleton curve in positive and negative loading direction deviates slightly, but this influence factor is not considered in finite element simulation.

4. Parametric Analysis

4.1. Axial Compression Ratio. Axial compression ratio is the ratio of the axial pressure of the column to the compressive strength of the entire section of the column. During the test, an axial pressure of 770 kN (axial compression ratio of 0.23) was applied to the column. Since the change in the axial compression ratio is not considered in the test, in this section, the influence of different axial compression ratios on the joint specimens was simulated and analyzed. The axial compression ratio n can be calculated according to

$$n = \frac{N}{N_u} = \frac{N}{f_y A_s + f_c A_c}, \quad (1)$$

where N represents the axial load, N_u is the ultimate bearing capacity of concrete-filled steel tube column, f_y is the yield strength of steel, f_c is the compressive strength of concrete, and A_s and A_s are the area of the steel tube and the core concrete, respectively.

Take the CFST-1 as an example. Figure 14 shows the load-displacement curves of joints with different axial compression ratios. The load-displacement curves of all

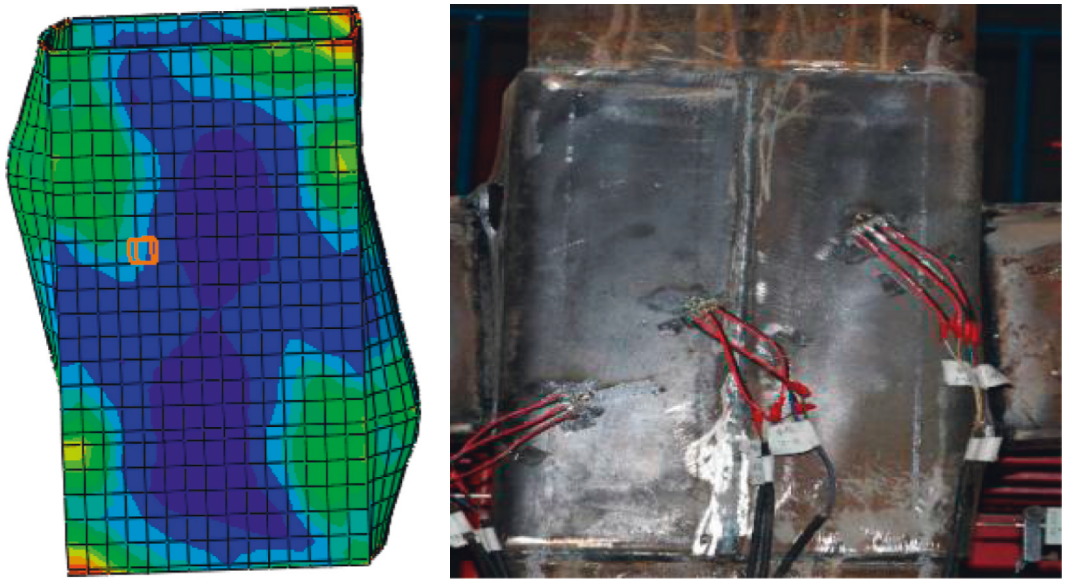

Figure 8: Failure mode.

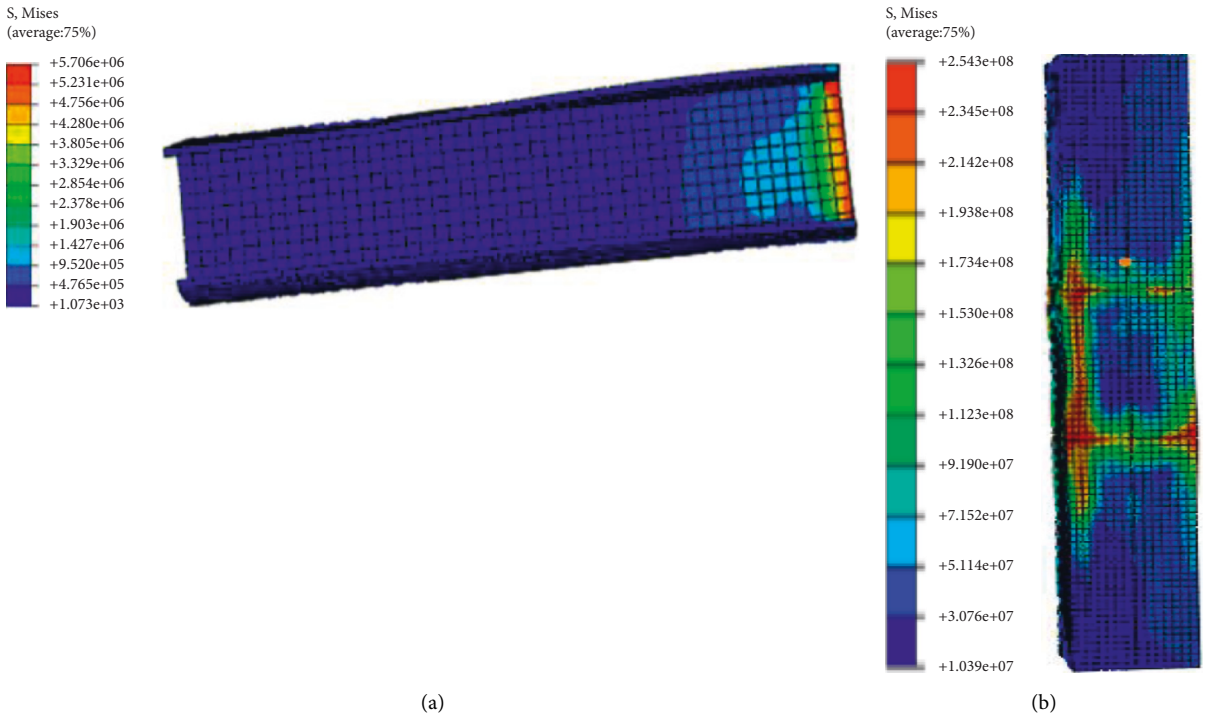

Figure 9: The stress distribution of steel beam and steel tube. (a) Steel beam and (b) steel tube.

parametric analyses below are obtained under monotonic loading. The initial stiffness is calculated by the slope of the elastic segment of the load-displacement curve. The slopes (initial stiffness) of the four curves are 1.116 ($n = 0.2$), 1.246 ($n = 0.4$), 1.408 ($n = 0.6$), and 1.334 ($n = 0.8$), respectively. It can be seen from the figure that, under the same boundary and loading condition, the joint still has a good bearing capacity, and the axial compression ratio is the main factor influencing the initial stiffness of the joint. When the axial compression ratio is smaller than 0.6, the initial stiffness of the joint is positively correlated with the axial compression ratio, but when this ratio exceeds 0.6, the initial stiffness of the joint will be negatively correlated with the axial compression

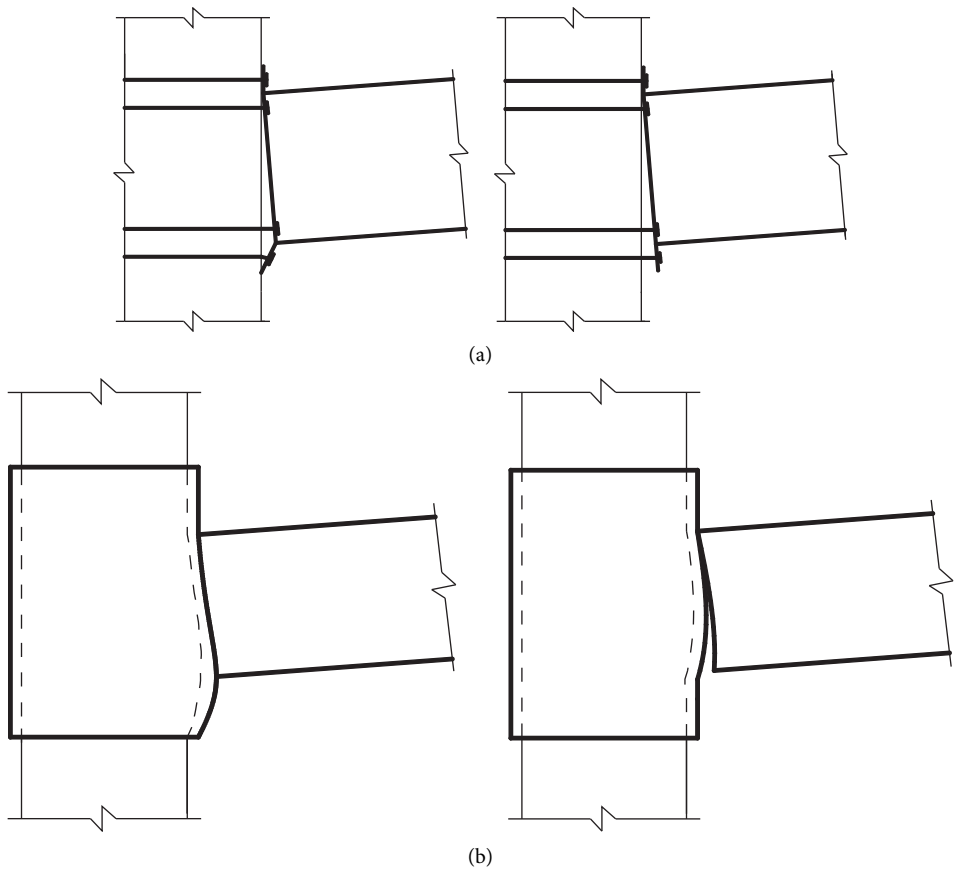

Figure 10: Comparison of failure modes of two semirigid joints. (a) Extended end-plate joint. (b) Sleeve joint.

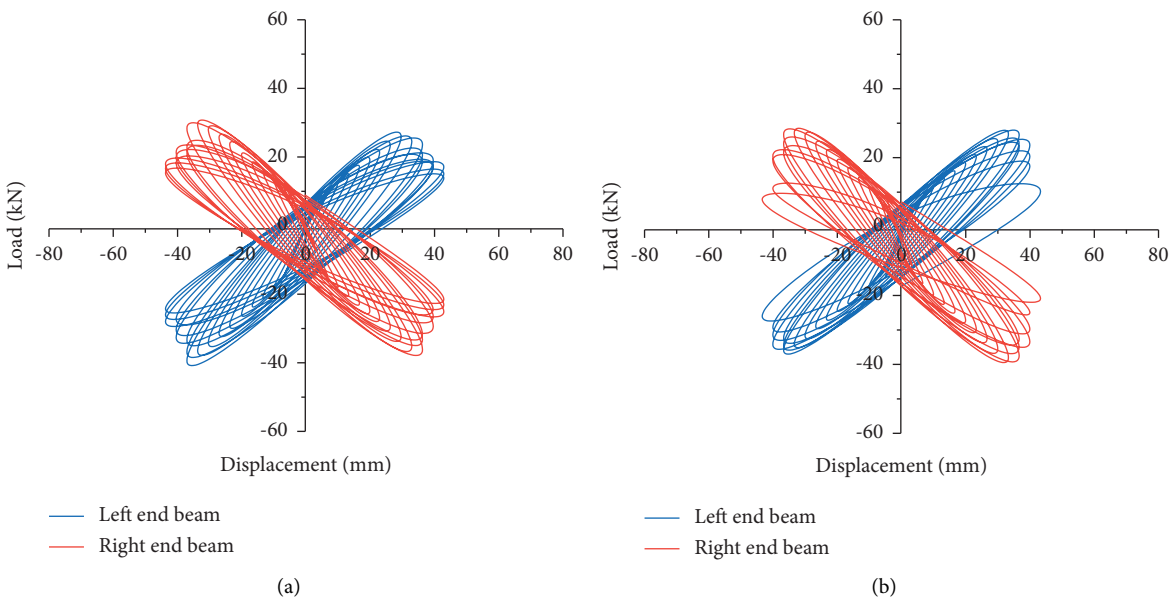

Figure 11: Continued.

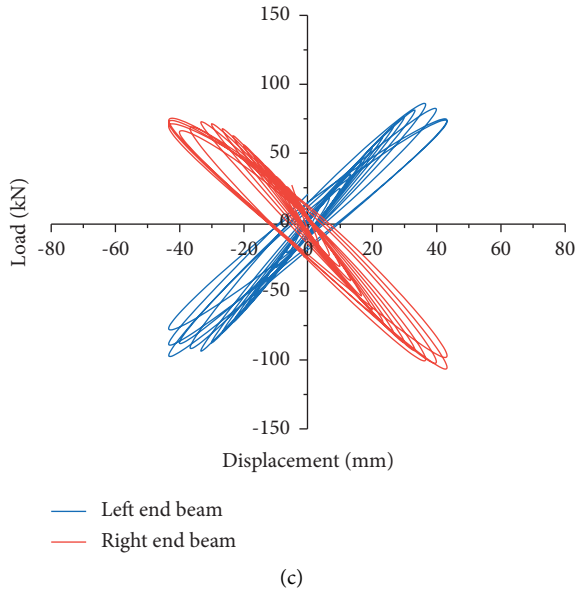

(c)

Figure 11: Load-displacement hysteretic curves of the beam end. (a) CFST-1, (b) CFST-2, and (c) CFST-3.

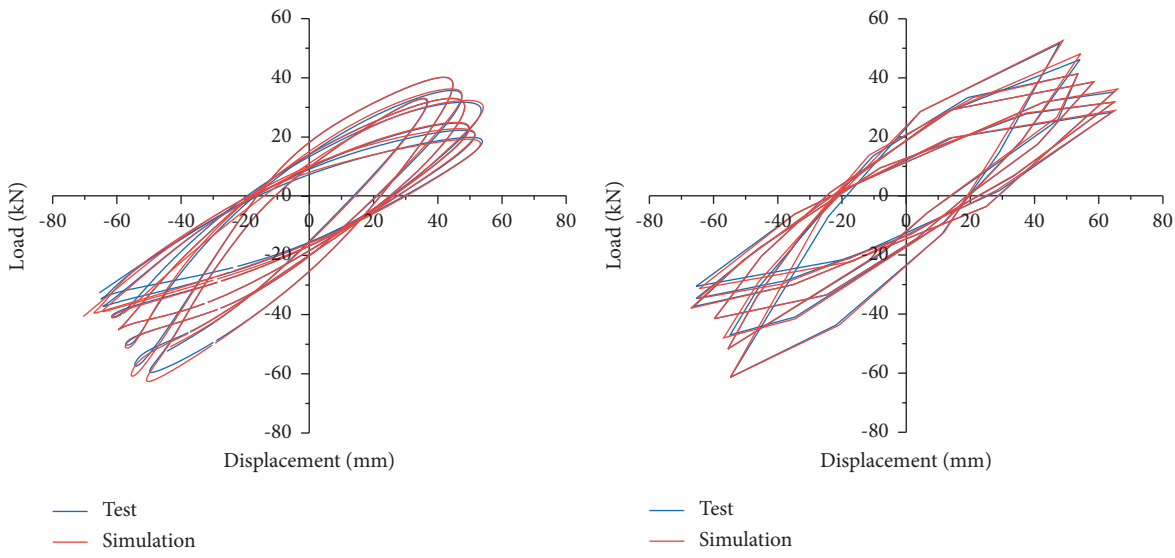

(a) (b)

Figure 12: Continued.

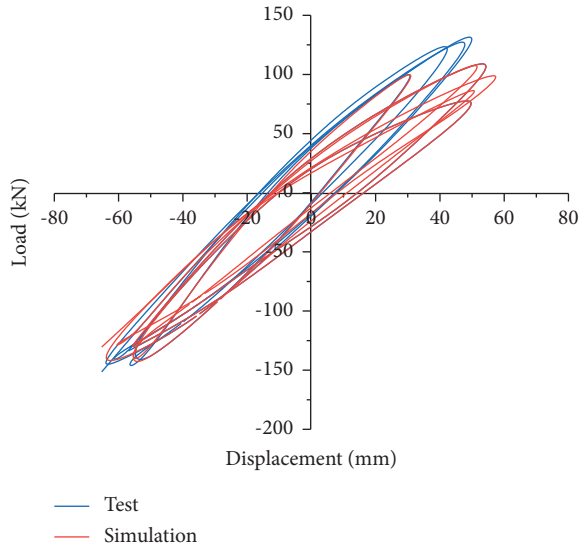

(c)

Figure 12: Comparison of hysteretic curves. (a) CSFT-1, (b) CFST-2, and (c) CFST-3.

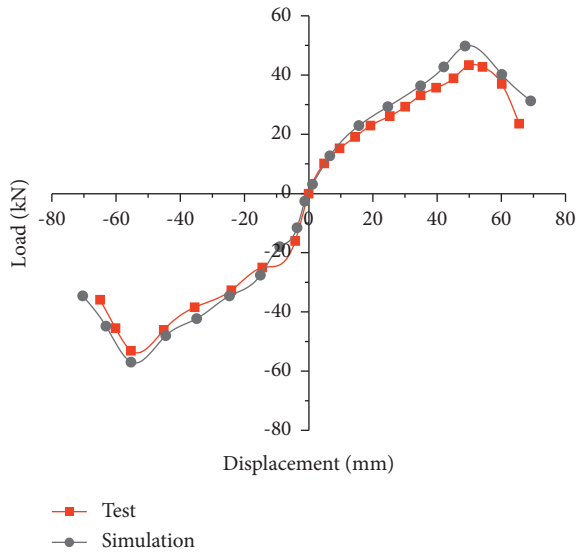

(a)

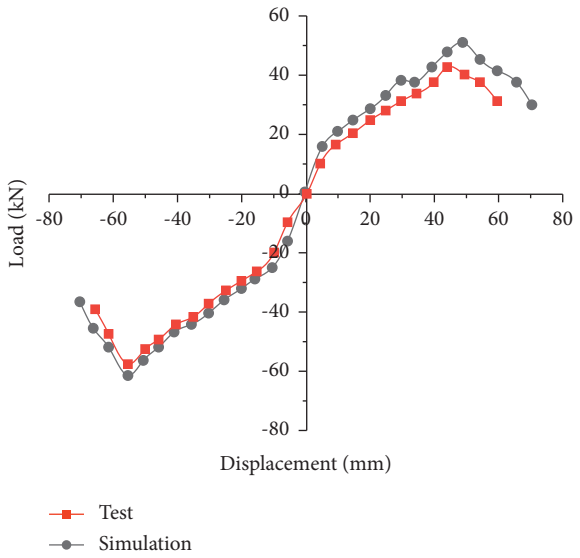

(b)

Figure 13: Continued.

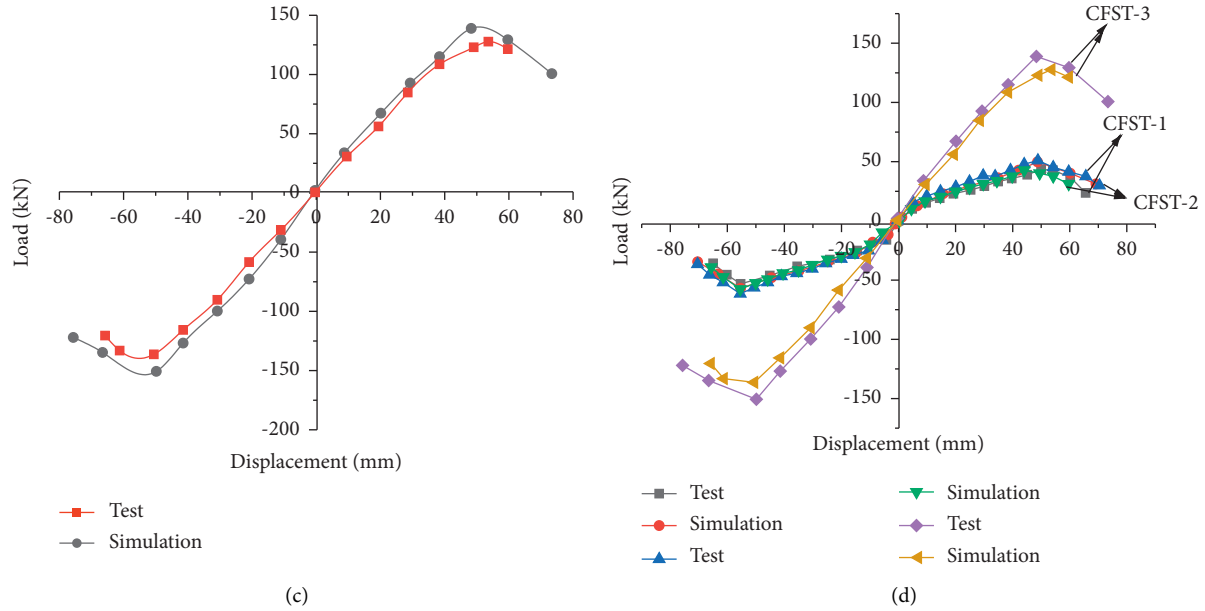

Figure 13: Comparison of skeleton curves. (a) CFST-1, (b) CFST-2, (c) CFST-3, and (d) comparison of skeleton curves under different parameters.

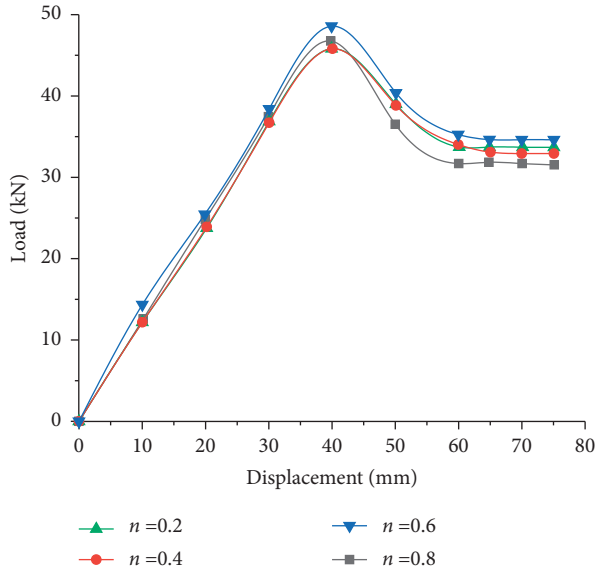

Figure 14: Load-displacement curves of joints with different axial compression ratios.

ratio. Therefore, it can be concluded that the joint achieves the optimal initial stiffness when the axial compression ratio $n = 0.6$.

It can be seen from Figure 15 that the hysteretic curves with the axial compression ratio $n = 0.2$ and $n = 0.4$ are almost the same, but the hysteretic curve with the axial compression ratio $n = 0.8$ shows an obvious "pinch" phenomenon, which indicates that it is affected by slippage. When the axial compression ratio exceeds 0.6, the energy dissipation capacity of the joint will be affected.

4.2. Influence of Concrete Strength Grade. The influence of different concrete strength grades on sleeve joints was analyzed, and the results are shown in Figure 16. It can be seen from Figure 16 that the concrete with higher strength bears more load in the later stage of loading so that the local buckling of steel tubular wall filled with concrete of higher strength is smaller than that filled with ordinary strength concrete. Thus, it can be concluded that increasing the concrete strength has a better effect that the yielding of the steel tube will occur later.

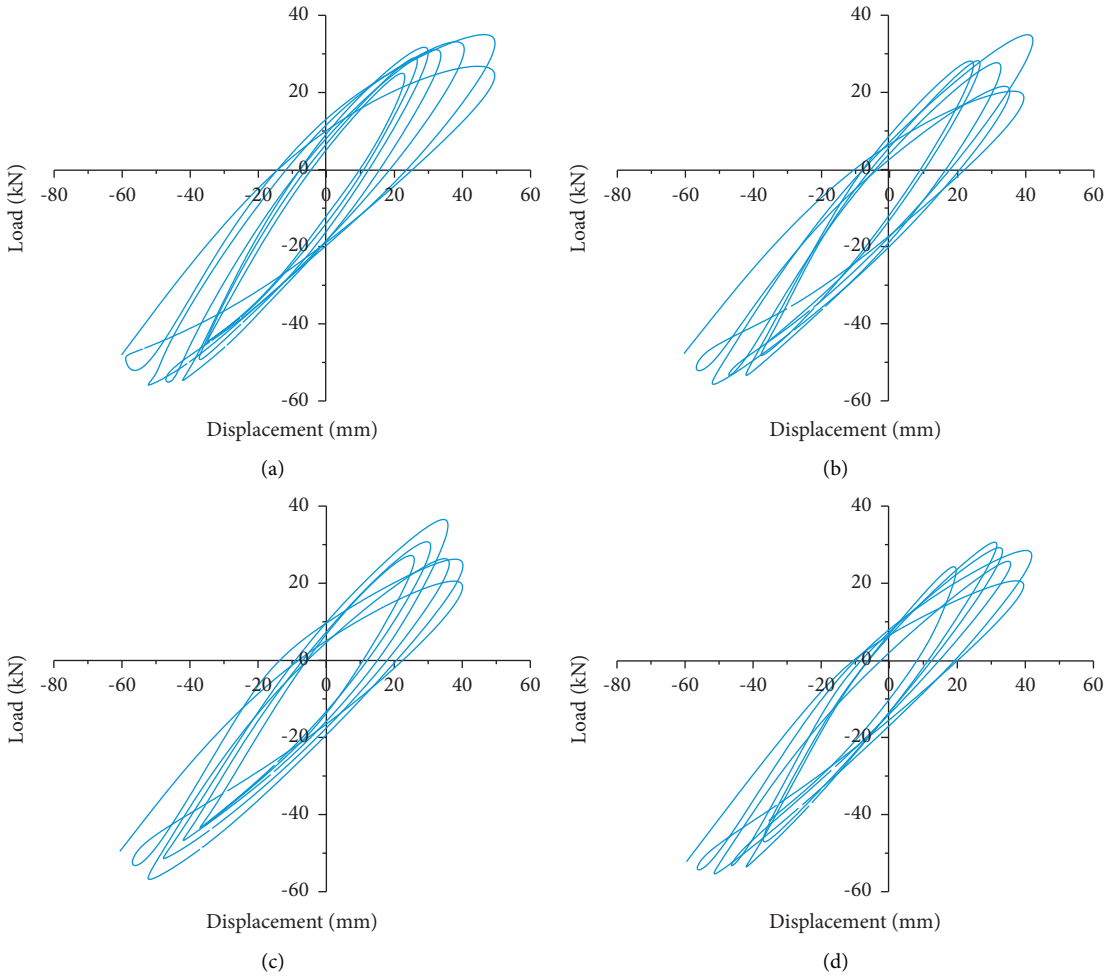

Figure 15: Hysteretic curves of joints with different axial compression ratios. (a) $n = 0.2$, (b) $n = 0.4$, (c) $n = 0.6$, and (d) $n = 0.8$.

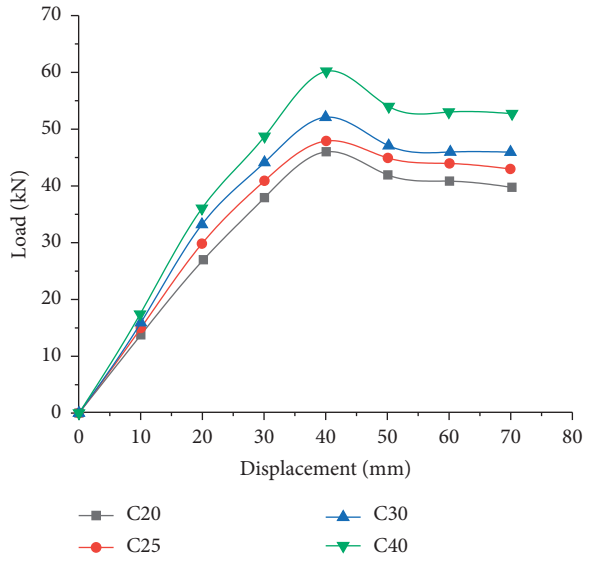

Figure 16: Load-displacement curves of joints with different concrete strength grades.

Figure 17 shows the hysteretic curves of joints with different concrete strengths. It can be seen from the figure that, compared with the initial hysteretic curve, the load increases by about 20% when the concrete strength increases. In addition, concrete strength has a significant influence on the overall elastic-plastic stage of the specimen, but before the elastic-plastic stage, the bearing capacity will not change significantly with increasing concrete strength.

4.3. Influence of Sleeve Thickness. Due to the limited test condition, only a few specimens were carried out, and the optimal sleeve thickness was not found. Therefore, in finite element analysis, the thickness of the sleeve was taken as 6 mm, 8 mm, 10 mm, 12 mm, and 16 mm for analysis and comparison, while other conditions remained constant. Figure 18 shows the load-displacement curves of joints with different sleeve thicknesses. As is observed, when the thickness of the sleeve is less than 10 mm, increasing the sleeve thickness can improve the stiffness and the ultimate bearing capacity. However, when the sleeve thickness exceeds 10 mm, the yield-bearing capacity and ultimate

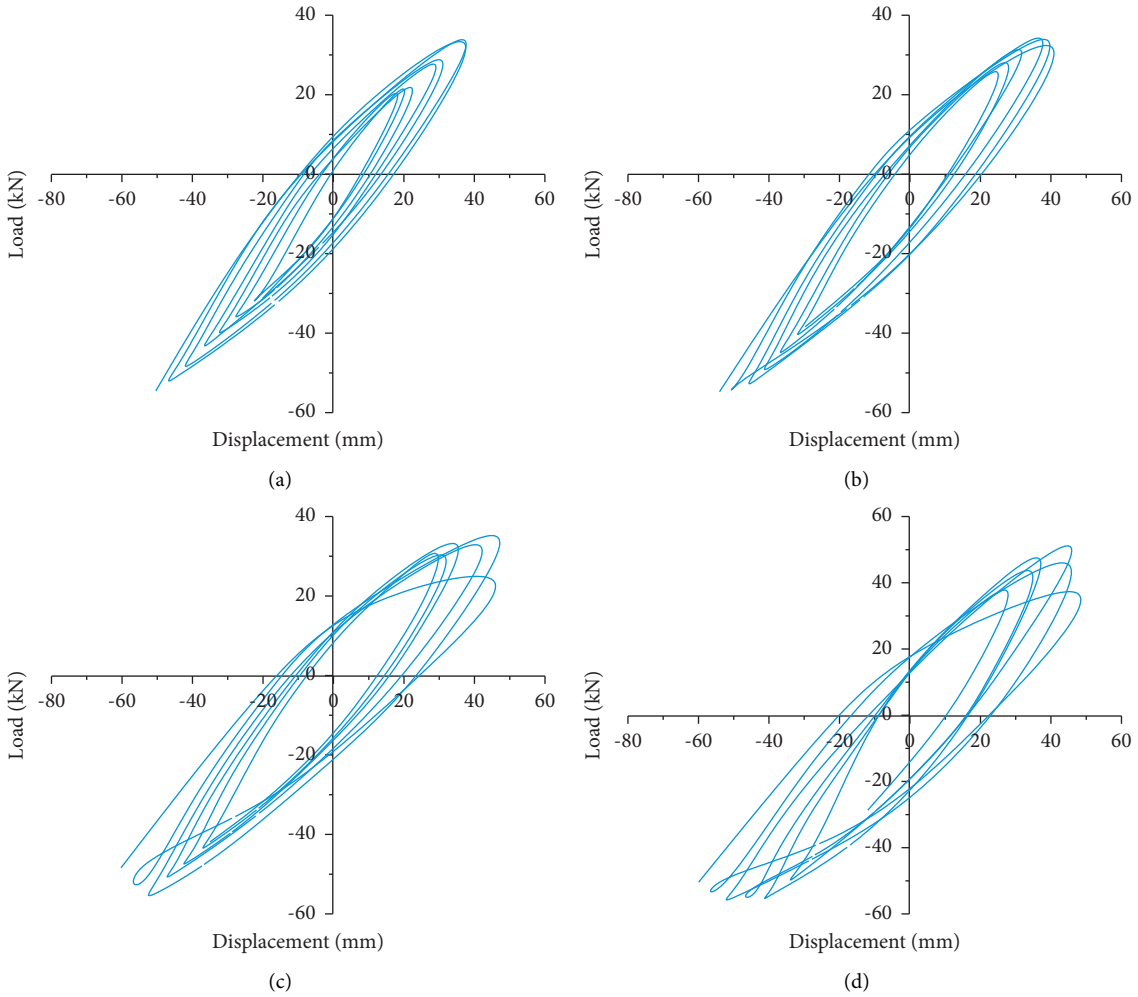

Figure 17: Hysteretic curves of joints with different concrete strength grades. (a) C20 concrete, (b) C25 concrete, (c) C30 concrete, and (d) C40 concrete.

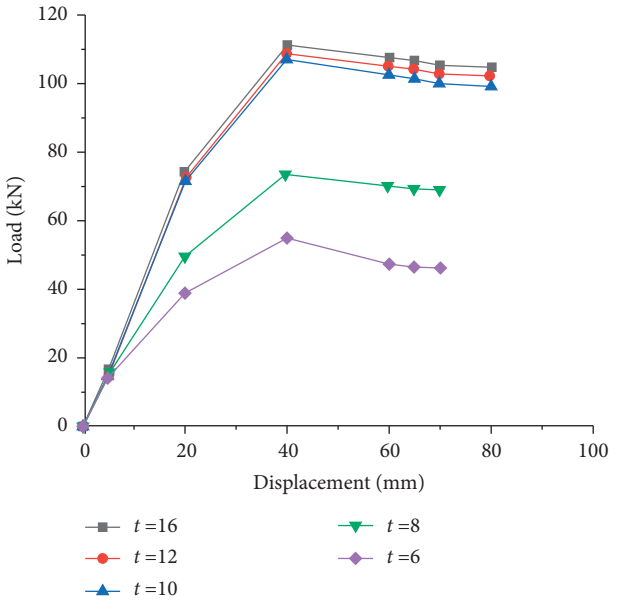

Figure 18: Load-displacement curves of joints with different sleeve thicknesses.

bearing capacity of the joints do not change significantly. The results show that when the thickness of the sleeve reaches 10 mm, the initial stiffness of the joint increases, but the increase is not obvious.

As shown in Figures 18 and 19, when the sleeve thickness exceeds 10 mm, the yield-bearing capacity and ultimate bearing capacity do not change significantly, and the hysteretic curves do not change much, indicating that the energy dissipation performance of the joint changes slightly. The results show that the seismic performance of joints can be improved with the increase of sleeve thickness, but the improvement effect is not obvious when the thickness exceeds a certain value. Moreover, when the thickness of the sleeve is less than 10 mm, the ultimate load increases significantly, which also leads to local buckling of the sleeve. Therefore, it is not recommended to increase the thickness of the sleeve without restriction when designing joints, which may result in unnecessary waste.

According to the test and finite element analysis, in order to meet the requirements that the joint strength should be higher than the members, the thickness of the sleeve needs to be greater than the thickness of the steel

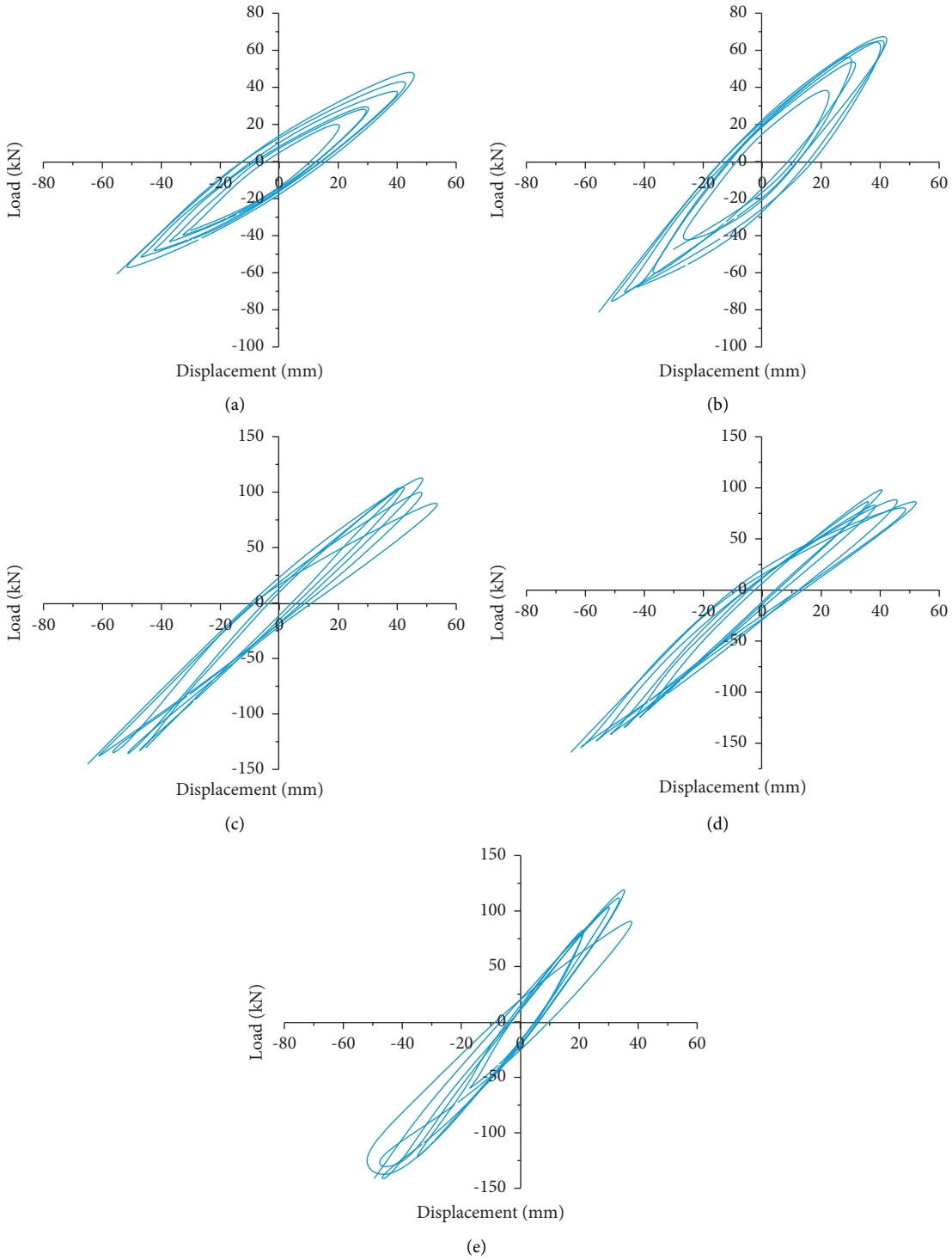

Figure 19: Hysteretic curves of joints with different sleeve thicknesses. (a) $t = 6$, (b) $t = 8$, (c) $t = 10$, (d) $t = 12$, and (e) $t = 16$.

tube to ensure that the sleeve does not buckle before the column-steel tube. However, when the thickness of the sleeve reaches a certain degree, the impact on the bearing capacity of the joint decreases. At this time, increasing the thickness of the sleeve will cause a waste of materials. Therefore, it is suggested that the ratio of sleeve thickness to steel tube thickness ranges from 1.0 to 1.25.

4.4. Influence of Sleeve Height. Take 2 times the beam height as the initial height of the sleeve. 1.2 times, 1.5 times, and 1.8 times the sleeve height were taken to compare with the initial height. Figure 20 shows the load-displacement curves of joints with different sleeve heights. As shown in the figure, when the height of the sleeve is increased while the sleeve thickness is unchanged, the initial stiffness of the sleeve joint slowly increases. Moreover, with the increase in sleeve

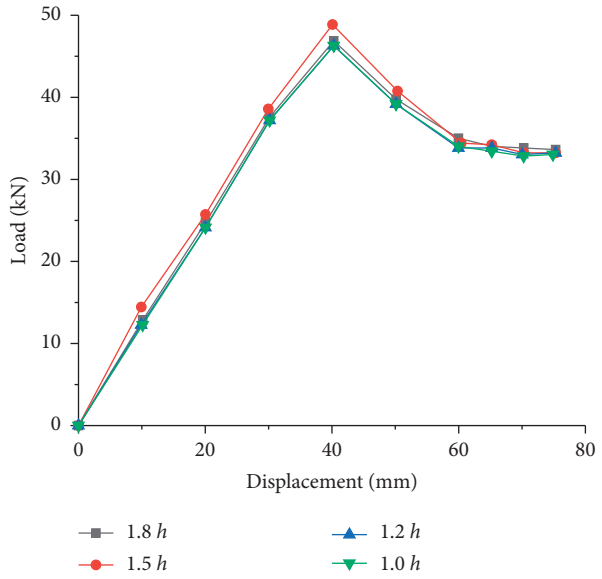

Figure 20: Load-displacement curves of joints with different sleeve heights.

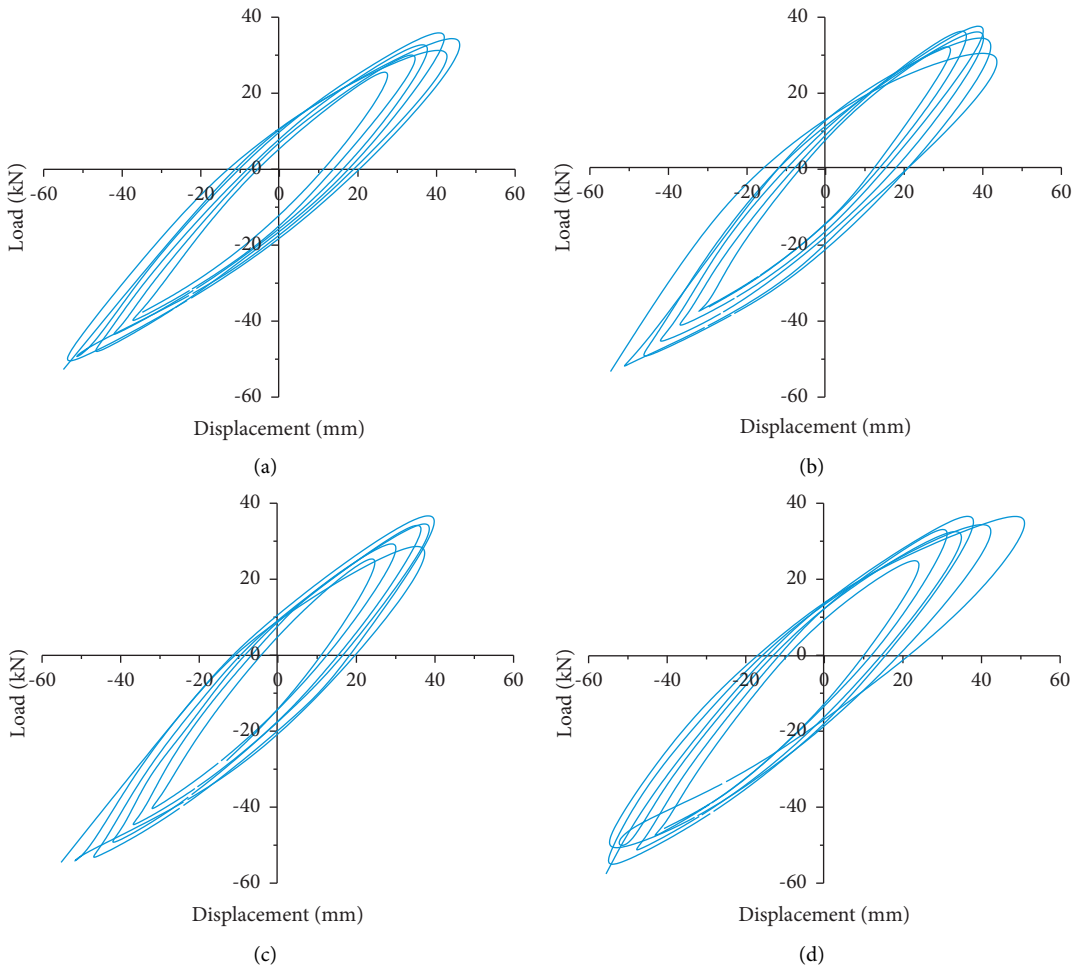

Figure 21: Hysteretic curves of joints with different sleeve heights. (a) 1 h, (b) 1.2 h, (c) 1.5 h, and (d) 1.8 h.

height, the ultimate load and ultimate displacement do not change significantly. Therefore, it is not economical to improve the bearing capacity of the joint by increasing the sleeve height.

Figure 21 shows the hysteretic curves of joints with different sleeve heights. By comparing the hysteretic curves of joints with each height, it is found that there is no significant change. However, as the height of the sleeve height increases, the shuttle shape becomes more obvious, and the hysteretic curve becomes fuller. It suggests that increasing the height can improve the energy dissipation capacity and ductility of the joints but has no significant effect on changing the ultimate bearing capacity and ultimate displacement. Moreover, as the height increases, the fabrication of sleeve joint specimens becomes more difficult. Therefore, the seismic requirements of joints can be met only by appropriately increasing the sleeve height.

5. Conclusions

In this paper, the method of numerical simulation analysis is used to design three concrete-filled steel tubal column-steel beam semirigid sleeve joints. The joint is composed of two steel plates and a sleeve welded together with the steel pipe column. The upper and lower flanges and webs at the end of the steel beam are welded by manual arc welding and completely welded on the sleeve. The validity of the finite element model is verified by comparison with experimental data, and the joints are subjected to low cyclic loading. The mechanical properties under different parameters are analyzed. Based on the analysis of this paper, the following conclusions can be drawn:

(1) The semirigid sleeve joint model is established by ABAQUS and compared with the hysteretic curves and skeleton curves of previous experiments, which verifies the applicability of the finite element model in simulating the seismic performance of the joint under low cycle load.

(2) The axial compression ratio and the height of the sleeve have little effect on the ultimate bearing capacity of the joint and have a small effect on the energy dissipation capacity. The design should be selected according to the economic principle.

(3) The thickness of the sleeve and the concrete strength grade are the main factors affecting the seismic performance of sleeve joints. When the thickness of the sleeve is increased or the concrete strength grade in the column is increased, the ductility and ultimate bearing capacity of the joint increase, and the energy consumption capacity is also improved.

(4) It is recommended that the thickness of the sleeve should be 1 to 1.25 times the thickness of the connecting steel tube. At the same time, according to the principle of economy, it is recommended that the height of the sleeve should not be greater than 2 times the height of the connecting steel beam.

Data Availability

The data used to support the findings of this study are included within the article.

Conflicts of Interest

The authors declare that they have no conflicts of interest.

Acknowledgments

This project was supported by the Natural Science Foundation of Heilongjiang Province (LH2019E005), Fundamental Research Funds for the Central Universities (2572017CB02), and National Science Foundation of China (51408106), which are gratefully acknowledged.

References

[1] L. H. Han, W. Bjorhovde, and R. Bjorhovde, "Developments and advanced applications of concrete-filled steel tubular (CFST) structures: Members," *Journal of Constructional Steel Research*, vol. 100, pp. 211–228, 2014.

[2] L. H. Han, Z. Tao, and W. D. Wang, "Advanced Composite and Mixed Structures: Testing," *Theory and design approach*, 2009.

[3] S. Gao, L. H. Guo, and Z. Zhang, *Anti-collapse performance of composite frame with spacial-shaped MCFST columns*, Engineering Structures, vol. 245, , 2021.

[4] S. Gao, M. Xu, F. Fu, and L. H. Guo, "Performance of bolted steel-beam to CFST-column joints using stiffened angles in column-removal scenario," *Journal of Constructional Steel Research*, vol. 159, pp. 459–475, 2019.

[5] S. Gao, "Nonlinear finite element failure analysis of bolted steel-concrete composite frame under column-loss," *Journal of Constructional Steel Research*, vol. 155, pp. 62–76, 2019.

[6] S. Gao and L. H. Guo, "Performance of circular bimetallic tube confined concrete slender columns under eccentric compression," *Archives of Civil and Mechanical Engineering*, vol. 21, no. 2, p. 40, 2021.

[7] X. H. Zhou, Z. Zhou, and D. Gan, "Analysis and design of axially loaded square CFST columns with diagonal ribs," *Journal of Constructional Steel Research*, vol. 167, Article ID 105848, 2020.

[8] D. Gan, Z. X. Li, T. Zhang, X. H. Zhou, and K. f. Chung, "Axial compressive behaviour of circular concrete-filled steel tubular stub columns with an inner bamboo culm," *Structures*, vol. 26, pp. 156–168, 2020.

[9] Oh and Ai-Roda, "T-Cleat connection to concrete-filled tubular internal columns," *Journal of Structural Engineering*, vol. 130, 2004.

[10] J. M. Ricles, S. W. Lu, and L. W. Lu, "Seismic behavior of composite concrete filled steel tube column-wide flange beam moment connections," *Journal of Structural Engineering*, vol. 130, no. 2, pp. 223–232, 2004.

[11] X. L. Yang, H. L. Wang, P. Dong, and Q. C. Ren, "Experimental research on the rectangular CFST column and H-section beam connections with through diaphragms," *Journal of Hebei University of Technology*, vol. 40, no. 6, pp. 79–82, 2011.

[12] X. L. Lv and X. P. Li, "Experimental study on ring-beam connections located outside the concrete- filled rectangular

steel tubular columns," *Journal of Building Structures*, vol. 24, no. 1, pp. 7–13, 2003.

[13] O. Mirza and B Uy, "Behaviour of composite beam-column flush end-plate connections subjected to low-probability, high-consequence loading," *Engineering Structures*, vol. 33, no. 2, pp. 647–662, 2011.

[14] Z. Y. Gao, H. Q. Li, and Z. C. Wang, "Mechanical performance of connect node between concrete filled square tubular column and H-steel beam," *World Earthquake Engineering*, vol. 31, no. 1, pp. 180–186, 2015.

[15] J. E. France and J. Buick Davison, "Moment-capacity and rotational stiffness of endplate connections to concrete-filled tubular columns with flowdrilled connectors," *Journal of Constructional Steel Research*, vol. 50, no. 1, pp. 35–48, 1999.

[16] Z. A. Huang, "A connection element for modelling end-plate connections in fire," *Journal of Constructional Steel Research*, vol. 67, no. 5, pp. 841–853, 2011.

[17] J. W. Hu, R. T. Park, and T. Park, "Mechanical models for the analysis of bolted T-stub connections under cyclic loads," *Journal of Constructional Steel Research*, vol. 78, pp. 45–57, 2012.

[18] L. H. Han, Z. Tao, and W. D. Wang, *Advanced Composite and Mixed Structures: Testing Theory and Design Approach*, Science Press, Beijing, China, 2009.

[19] L. H. Han, *Concrete Filled Steel Tubular Structures––Theory and practice*, Science Press, Beijing, China, 2007.

[20] Gb/T 2975-2018, *Steel and steel products––location and preparation of samples and test pieces for mechanical testing*, China Standards Press, China, 2018.

[21] L. L. Sun, Z. Q. Liang, Q. S. Wang et al., "Seismic response on T-head square-neck one-side bolted endplate connection of beam to square tubular column," *Engineering Structures*, vol. 246, Article ID 113077, 2021.

[22] L. L. Sun, Z. Q. Liang, M. Cai et al., "Seismic behaviour of TSOBs bolted I-beam to hollow section square column connection with inner stiffener," *Journal of Building Engineering*, vol. 51, Article ID 104260, 2022.

[23] J. B. Li and X. Li, "Realization of strong column-weak beam failure mode for concrete-filled square steel tubular frame structure," *Advanced Materials Research*, vol. 446-449, pp. 424–428, 2012.

[24] Y. Z. Yin and Y. Zhang, "Research on the seismic behavior of concrete-filled steel tubular column and steel beam joint," *Applied Mechanics and Materials*, vol. 204-208, pp. 2528–2532, 2012.

[25] Gb/T 228-2010, *Metallic materials––Tensile testing––Method of test at ambient temperature*, China Standards Press, China, 2002.